



Design, fabrication and characterization of terahertz five-band metamaterial absorber

A ELAKKIYA[✉], SRIGITHA S NATH* and M VANITHA

Department of ECE, Saveetha Engineering College, Sriperumbudur Taluk, Kanchipuram, Chennai 602 105, India

*Corresponding author. E-mail: hod.ece@saveetha.ac.in

MS received 9 May 2022; revised 2 January 2023; accepted 24 January 2023

Abstract. This research presents the simulation, fabrication, and measurement of a new terahertz (THz) metamaterial absorber (MMA). Copper and polyimide are the materials used in this project. The polyimide substrate is sandwiched between the two copper conductor layers. Theoretical results reveal that the absorber has five distinct and significant absorption peaks at 0.994, 0.97, 0.947, 0.904 and 0.892 THz, respectively, with absorption rates of 94%, 99.9%, 99.9%, 97%, and 92%. The electric field, magnetic field, and surface current distributions are used to investigate the structure's physical mechanism. The incident and polarisation angles of the structure are modified from 0 to 90 degrees to examine the insensitive behaviour of the incident angle and polarisation angle. Laser micromachining and terahertz time-domain spectroscopy are used to build and examine the structure. This work is compared with previous works. It has numerous scientific and sensory applications.

Keywords. Metamaterial absorber; laser micromachining; terahertz time-domain spectroscopy.

PACS Nos 81.05.Xj; 78.67.Pt; 87.50.U

1. Introduction

Perfect lensing, invisibility, negative refractive index, cross-polarization conversion, perfect absorption and asymmetric transmission are all properties of metamaterials [1]. The structure, rather than the composition, determines the properties of these materials. Because of their unique properties, metamaterials are excellent electromagnetic wave absorbers. Metamaterial filters, multiband metamaterial absorbers, broadband metamaterial absorbers and cloaking devices have all been shown to change electromagnetic waves from microwaves to visible wavelengths [2–5]. In 2008, Landy *et al* [6] proposed the first-ever MMA. A splitting resonator and metallic cut wires were used to create a metamaterial that achieved single-point absorption when a dielectric sheet was placed between them. Following that, several researchers introduced a large variety of absorbers. Sensors, filters, switches and modulators, among other uses, have all made use of these absorbers [7, 8]. Many efforts have been done by researchers [9–11] to broaden the absorption curve from microwave, infrared, to terahertz until the optical area. They are all inefficient, though, because they have limited frequency ranges and do not allow for some

practical uses. Researchers generally used four ways to improve absorption rate and bandwidth range. In the first method, a variable-sized resonator is employed in a single unit cell to produce multi-band functioning. In the second technique, several material layers are stacked within a single unit cell. The third strategy is a hybrid of the first and second strategies. Doped composite materials are used in the final procedure [12–14].

However, there are two major drawbacks to these approaches. The first is that the unit structure has a huge unit cell size difficulty, and the second is that the stacked structure has technical challenges with misalignment or fabrication errors. The important tendency of shrinking and simplification is not met by these designs. As a result, simple planar structures are required for multiband and broadband absorbers. Cao *et al* [15], Shen *et al* [16], Ben-Xin *et al* [27], Huang *et al* [18] and Wang *et al* [19] for example, have shown multi-band absorbers based on several different-sized unit elements in a single super-unit cell structure. He *et al* [20], Hu *et al* [21] and Zhu *et al* [22] demonstrated broadband absorbers by stacking numerous different shapes and sizes of metallic patterns. These structures, on the other hand, are incredibly

difficult to inspect, posing enormous simulation and construction issues. Previous experiments required a lot of layers to accomplish multiple band absorption. A single-designed resonator with only one substrate layer yielded multi-band absorption responses in this experiment.

The highlights of the proposed metamaterial absorber are, achieving five different absorption peaks above 90% absorption rate for all the five frequencies at both simulation and fabrication results without overlapping. The structure is very easy to design in CST Microwave Studio Software. By carefully engineering the electric and magnetic resonances, it is possible to create metamaterials with perfect absorption. In an MMA, simultaneous electric and magnetic resonances are required to establish impedance matching ($Z = Z_0$). An electric or magnetic metamaterial with a single resonance will have an impedance that is significantly different from that of empty space. As a result, there would be no unity absorber. The top copper layer uses the incident plane wave to produce an electric response. The magnetic response is produced and the transmission wave is zero on the bottom copper metallic plane.

2. Design and materials

Figure 1(a) shows the three layers of the designed five-band terahertz metamaterial absorber, which include a copper metal ground layer at the bottom, a dielectric substrate layer in the middle, and an octagon patterned resonator layer at the top. The front view of the absorber with dimensions is shown in figure 1(b). The structure's optimal parameters are listed in Table 1. From the table, $(r_1 \times r_2)$ represents the inner (160 μm) and outer radius (240 μm) of the octagon. The substrate is a polyimide with a dielectric loss tangent ($\tan \delta$) of 0.0027 and a permittivity (ϵ_0) of 3.5. The thickness of the copper layer is 0.5 μm with a frequency-insensitive conductivity of $\sigma = 5.8 \times 10^7$ Siemens/m [23]. Unlike prior MMAs, the proposed MMA can achieve five unique absorption curves with a single resonator. The absorption behaviour and structural efficiency are demonstrated using commercially available Computer Simulation Technology (CST) microwave studio software. In the x and y directions, the periodic boundary conditions were used in the simulations, with a totally matched open layer boundary condition in the z plane. The X and Y borders are used on four sides of a single unit cell in unit cell boundary conditions. It has several size restrictions. An open space, like a free space, has a boundary condition. Waves can travel past this barrier with little reflection. This open barrier is created by the Floquet port.

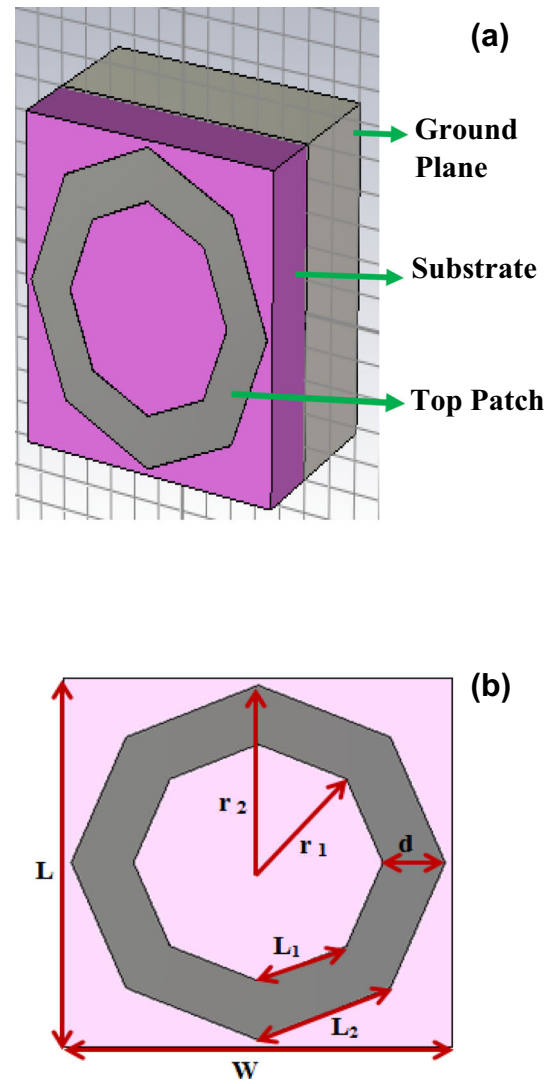


Figure 1. (a) Perspective view (3D) of THz MMA. (b) A unit cell of the THz MMA (polyimide in pink, copper in black).

Table 1. Parameters of the designed MMA structure.

Parameters	Values (μm)
Substrate width and length ($W \times L$)	(500 \times 500)
Radius of the octagon ($r_1 \times r_2$)	(160 \times 240)
Substrate height (h)	125
Distance (d)	80
Edge length of the inner octagon (L_1)	0.12
Edge length of the outer octagon (L_2)	0.18

3. Absorption mechanism

Figure 2 shows the absorption curve of the five-band terahertz metamaterial absorber. There are five absorption curves with absorption rates of 94%, 99.9%,

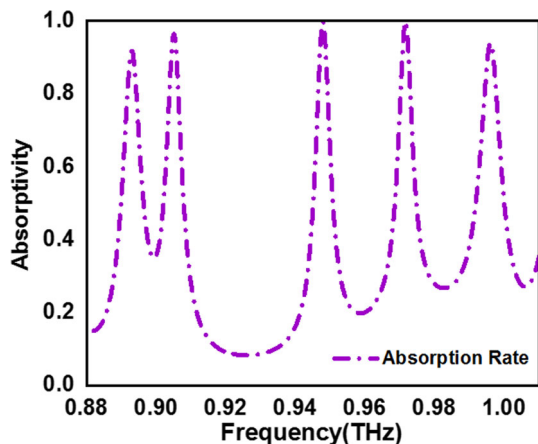


Figure 2. Absorptivity of THz MMA.

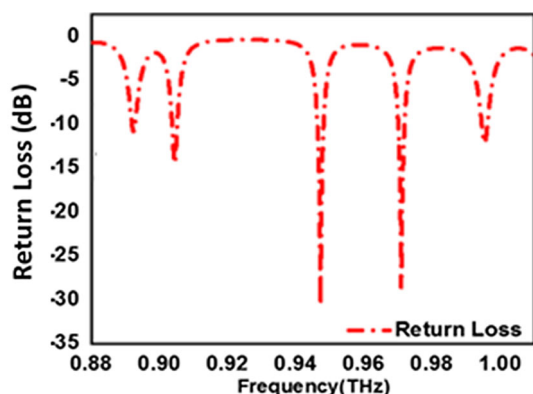


Figure 3. Return loss characteristics of five-band MMA.

99.9%, 97% and 92% in the simulated findings at 0.994, 0.97, 0.947, 0.904 and 0.892 THz, respectively. This five-band terahertz absorber peak is narrower than

the previous MMAs. Figure 3 depicts the suggested absorber’s return loss characteristic. The return loss of polyimide-based absorber structures is less than -10 dB, making them excellent for near-unity absorption. The absorption is calculated by, $A = 1 - R(\omega) - T(\omega)$, where T is the transmission, A is the absorption, ω is the angular frequency and R is the reflection. Since the thickness of the ground metal layer is larger than its skin depth, $T(\omega)$ goes to zero. The impedance-free space can be constructed to match the impedance of the absorber at a certain frequency, resulting in a reflection coefficient of zero and a higher possibility of obtaining an absorption value of one.

4. Simulated response at different incident angles (θ) and polarization angles (ϕ)

The MMA must have constant absorption performance for different incidence and polarisation angles in actual applications. The metamaterial absorber’s polarisation and oblique incidence angle values are numerically analysed. Figures 4(a) and (b) depict the simulated absorbance of the proposed metamaterial absorber, where (θ) and (ϕ) are changed from 0 to 90 degrees across the entire frequency range of interest (0.88 to 1.02 terahertz).

Because of the symmetric nature of the structure, the absorption and resonant frequency did not change when the θ and ϕ values were changed. As a result, the proposed MMA possesses outstanding polarization-independent absorption properties. This is due to the intended MMA’s unit cell structure.

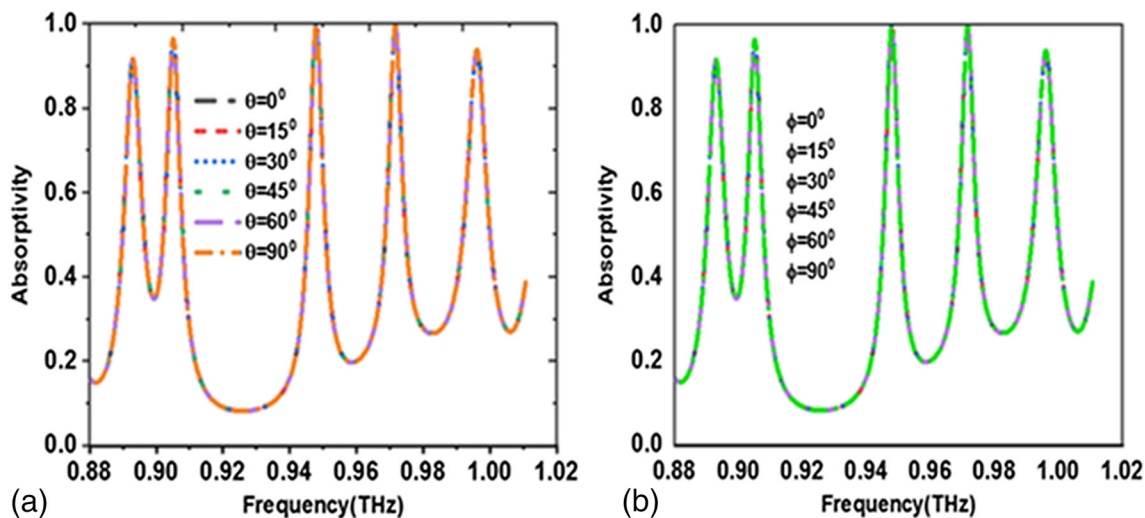


Figure 4. Absorbance characteristics of the structure for (a) different incident angles and (b) different polarization angles under normal incidence conditions.

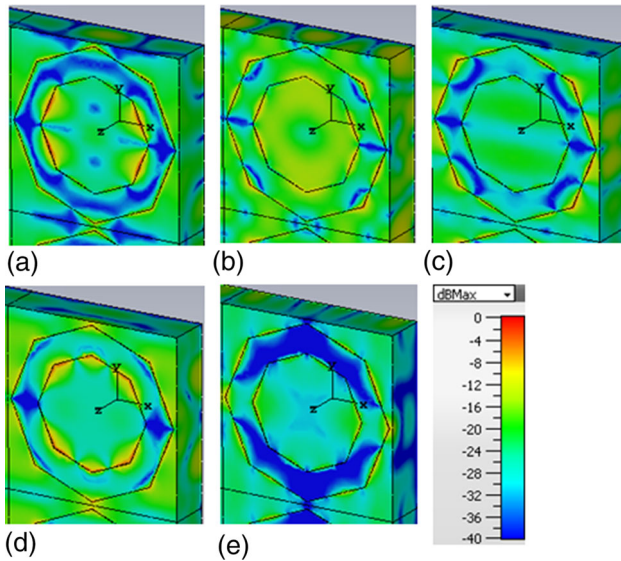


Figure 5. Distributions of the E -field at frequencies of (a) 0.892, (b) 0.904, (c) 0.947, (d) 0.97 and (e) 0.994 THz.

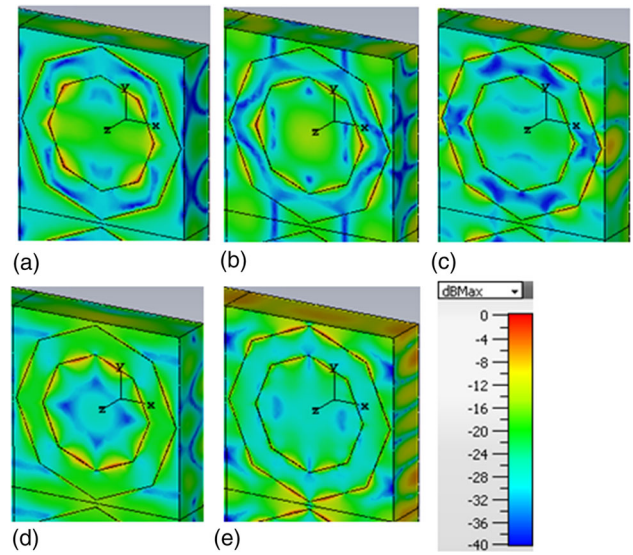


Figure 6. Distributions of the M -field at frequencies of (a) 0.892, (b) 0.904, (c) 0.947, (d) 0.97 and (e) 0.994 THz.

5. Electric and magnetic field distributions

The electric field distributions at different resonance frequencies are shown in figures 5(a)–(e) to investigate the physical mechanism of the proposed five-band terahertz for frequencies of 0.904 THz and 0.97 THz. The field appears concentrated on the polyimide layer and some locations in the patch resonated absorber structure when the absorption frequency is 0.947 THz and 0.994 THz. Figures 6(a)–(e) illustrate the magnetic field distributions of the proposed five-band terahertz metamaterial absorber. The absorption curve is concentrated across the patch structure and the polyimide dielectric layers, as illustrated in figures 6(a), (d) and (e). The magnetic field distribution on the full substrate layer and some spots in the top absorber structure are concentrated at frequencies of 0.904 THz and 0.947 THz. The field intensity determines the physical significance of the electric and magnetic field distributions at the associated frequency values. This field intensity is utilised to determine the electric and magnetic metamaterial absorber. The initial absorption curve is concentrated on the polyimide layer and some spots in the resonant structure, as shown in figure 5(a). The field distributions occur at the entire patch structure and the surface of the dielectric substrate field distribution is greatest at the metamaterial absorber structure.

6. Surface current distributions

Figure 7 shows the surface current distributions on the top radiating metallic surfaces of the proposed MMA at

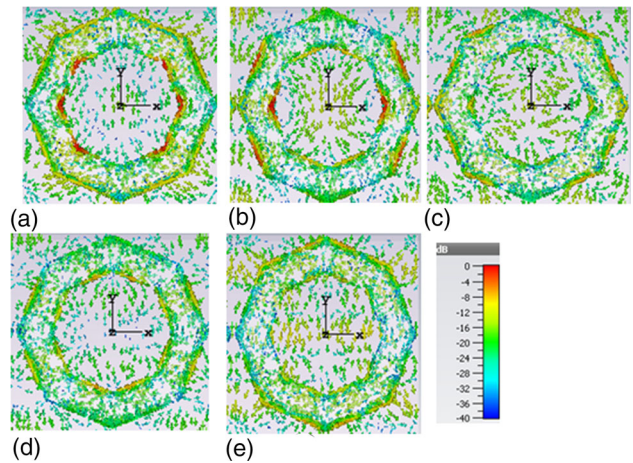


Figure 7. Distributions of the surface current at frequencies of (a) 0.892, (b) 0.904, (c) 0.947, (d) 0.97 and (e) 0.994 THz.

five different frequencies: (a) 0.892, (b) 0.904, (c) 0.947, (d) 0.97 and (e) 0.994 THz. In some places of the radiator's surface, oppositely directed currents have been discovered. It generates substantial charge build-up for such regions that take opposite currents, resulting in an electric resonance mechanism. As a result, the incident EM wave is heavily absorbed by these two resonators at all five frequencies.

7. Fabrication and characterization results of five-band THz MMA

There are two primary processes in the fabrication process. The initial stage was to deposit a copper metal over

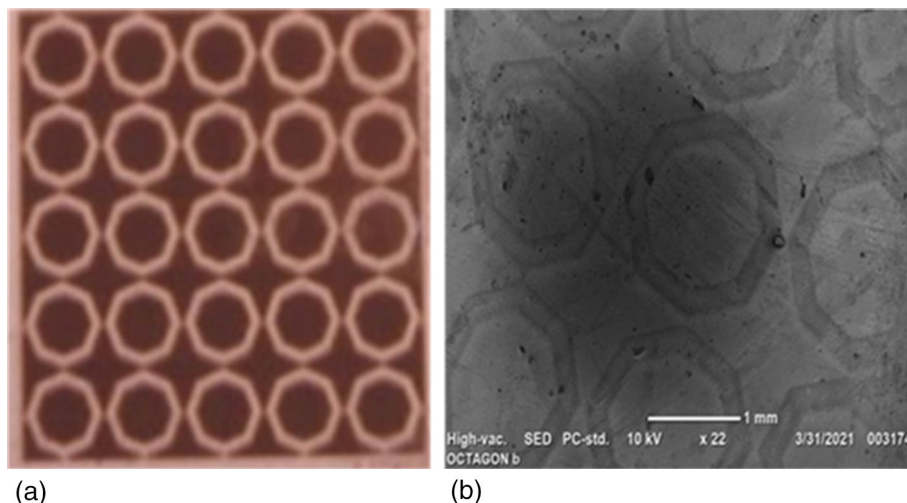


Figure 8. (a) Optical microscopic image of the femtosecond fiber laser fabricated proposed metamaterial. (b) Scanning electron microscopic image periodic configuration.

the polyimide substrate with a DC magnetron sputtering unit model at a pressure of 2×10^{-5} bar and a temperature of 250 °C. The material is then abated from the target material using a 350 fs, 800 kHz fiber laser. Following the fabrication procedure, the material’s ablated area is investigated using optical and scanning electron microscopic imaging, as illustrated in figures 8(a) and (b). The measurement results for the suggested MMA structure are shown in Fig. 9. The THz-TDS spectroscopy is employed to characterise the constructed array structure for the terahertz frequency range. With the use of terahertz laser pulses, terahertz time-domain spectroscopy is utilised to generate the electrical and optical properties of the material. The THz-TDS typically spans the spectral region between 0.1 and 3 THz. This method is employed in numerous fields, including biomedical imaging, the pharmaceutical sector, security screening procedures, etc. The terahertz pulses are produced by a commercial BATOP source-based Photo Conductive Antenna (PCA) THz detector made of a ZnTe crystal and based on the EO sampling method. The incident beam is divided into two halves by a beam splitter; one beam is utilised as a pump to produce terahertz waves, and another beam serves as a probe to detect them. Two parabolic reflectors collimate the THz wave both before and after it passes through the test sample. The polarisation rotation of the probe beam, which is detected using a Wollaston prism, was induced by the incident THz electric field on the detecting side. Between the pump THz and the probe beams, a delay stage has been added. A plexiglass enclosure has been placed over the complete setup to prevent environmental and chemical disruptions, and a nitrogen atmosphere has been generated.

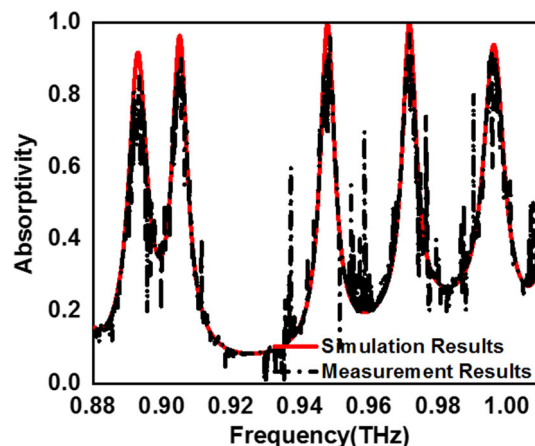


Figure 9. Absorption rate characteristic of the fabricated MMA using THz-TDS.

The amplitude variance of a copper and polyimide material sample may show the outcomes of inhomogeneity. The optical and electronic noise as well as the laser intensity changes during the laser micromachining process, which are the common causes of output resolution errors. The environmental factors have an impact on the samples while they are being measured. As a result, the calculated data contains some noise.

8. Conclusion

CST Microwave Studio Software is used to develop and mathematically analyse a five-band THz MMA. It just has three layers and has absorptivity values of 92, 97, 99.9, 99.9 and 94%. Table 2 compares the planned five-band MMA results with those of previous studies. The

Table 2. Comparison of the proposed absorber structure with previous multi-band absorbers.

Ref.	Absorption peaks	Obtained methods: Coplanar (C), stacked (S)	Number of elements	Materials used
[24]	1	C	4	Silver, glass
[25]	2	C + S	2	Au, polyimide, Si
[26]	3	C + S	3	Au, polyimide, Si
[24]	4	C + S	2	Au, polyimide, Si
[27]	5	C	3	Au, polyimide
[28]	6	S	1	Au, polyimide, Si
[29]	7	–	1	Cu, polyimide
[30]	8	–	1	Au, GaAs
[31]	15	C	25	Cu, GaAs
This work	5	–	1	Cu, polyimide

terahertz time-domain spectroscopy apparatus is used to characterise MMA absorption, and the femtosecond laser micromachining method is used to fabricate MMA. The optical and SEM pictures are used to examine the produced sample. The resonance variation could be produced by tiny form changes in the created structure due to the laser micromachining operation. The terahertz MMA micro machine using a femtosecond laser has precise and smoothed ablated zones, making it ideal for use in medical applications and bio-sensing applications.

References

- [1] P H Siegel, *IEEE Trans. Microw. Theory Techn.*, **50**, 910 (2002)
- [2] D R Smith, J B Pendry and M C K Wiltshire, *Science* **305**, 788 (2004)
- [3] C D Stoik, M J Bohn and J L Blackshire, *Opt. Express*, **16**, 17039 (2008)
- [4] C Sabah, B Mulla, H Altan and L Ozyuzer, *Pramana – J Phys.* **91**, 17 (2018)
- [5] M Tonuchi, *Nat. Photonics* **1**, 97 (2007)
- [6] N I Landy, S Sajuyigbe, J J Mock, D R Smith and W J Padilla, *Phys. Rev. Lett.* **100**, 207402 (2008)
- [7] M R Soheilifar and F B Zarrabi, *Opt. Quant. Electron.* **51**, 155 (2019)
- [8] H Zhou, F Ding, Y Jin and S He, *Prog. Electromagn. Res. C*, **119**, 449 (2016)
- [9] B-X Wang, G-Z Wang and L-L Wang, *Plasmonics* **11**, 523 (2016)
- [10] B Ashvanth and S Kanimozhi, *Pramana – J Phys.* **95**, 193 (2021)
- [11] Y Cheng, Y Zou, H Luo, F Chen and X Mao, *J. Electron. Mater.* **48**, 3939 (2019)
- [12] M Pu, M Wang, C Hu, C Huang, Z Zhao, Y Wang and X Luo, *Opt. Express* **20**, 25513 (2012)
- [13] H Liu, K Luo, S Tang, D Peng, F Hu and L Tu, *Materials*, **11**, 2590 (2018)
- [14] X Chen, Z Wu, Z Zhang and Y Zou,
- [15] S Cao, W Yu, T Wang, H Shen, X Han, W Xu and X Zhang, *Opt. Mat. Expr.*, **4**, 1876 (2013)
- [16] G Shen, M Zhang, Y Ji, W Huang, H Yu and J Shi, *AIP Advances*, **8**, 075206 (2018)
- [17] Q Bian, X Yu, B Zhao, Z Chang and S Lei, *Opt. Laser Technol.* **45**, 395 (2013)
- [18] L Huang, D R Chowdhury, S Ramani, M T Reiten, S N Luo, A J Taylor and H T Chen, *Opt. Lett.* **37**, 154 (2012)
- [19] B X Wang, X Zhai, G Z Wang, W Q Huang and L L Wang, *IEEE Photonics J.* **7**, 1 (2015)
- [20] Y He, Q Wu and S Yan, *Plasmonics*
- [21] D Hu, H Wang and Q Zhu, *IEEE Photonics J.* **8**, 1 (2016)
- [22] J Zhu, Z Ma, W Sun, F Ding, Q He, L Zhou and Y Ma, *Appl. Phys. Lett.* **105**, 021102 (2014)
- [23] W Withayachumnankul and D Abbott, *IEEE Photonics J.* **1**, 99 (2009)
- [24] B R Sangala, A Nagaraja, P Deshmukh, H Surdi, V G Achanta and S S Prabhu SS, *Pramana – J Phys.* **94**, 2 (2020)
- [25] G Shen, M Zhang, Y Ji, W Huang, H Yu and J Shi, *AIP Adv.* **8**, 075206 (2018)
- [26] S Liu, H Chen and T J Cui, *Appl. Phys. Lett.* **106**, 151601 (2015)
- [27] B-X Wang, Y He, P Lou, W-Q Huang and F Pi, *Results Phys.* **16**, 102930 (2020)
- [28] W Wang, K Wang, Z Yang and J Liu, *J. Phys. D: Appl. Phys.* **50**, 13, 135108 (2017)
- [29] A Elakkiya, S Radha and B S Sreeja, *Circuit World*, **47**, 400 (2021)
- [30] V K Verma, S K Mishra, K K Kaushal, V Lekshmi and S Sudhakar *Plasmonics* **15**, 75 (2020)
- [31] D Hu, H Wang, J Zhang, Z Wang, X Zhang and Q Zhu, *J. Phys. D: Appl. Phys.* **53**, 275108 (2020)